AD 296 147

STANFORD RESEARCH INSTITUTE
MENLO PARK, CALIFORNIA

February 1, 1963

Progress Report No. 23
For the period November 1 to January 31, 1963

TUNGSTEN AND ROCKET MOTORS

SRI Project No. PMU 2785
Contract NOrd-18619

Prepared for:
Special Projects Office
Department of the Navy
Bureau of Naval Weapons
Washington 25, D. C.

Introduction

The current project, a continuation of Task II, NOrd-18619, concerns the use of tungsten in solid propellant rocket motors and involves two main areas of interest. The first area, tungsten erosion, is being studied under simulated exhaust conditions by means of a specially constructed plasma arc erosion apparatus. The second area deals with the effects of thermal shock on tungsten and includes an experimental study and theoretical analysis of the problem.

Erosion Studies

Erosion of Ag-infiltrated W by CO_2

Three Ag-infiltrated W specimens were received from Aerojet-General Corporation. A CO_2-erosion run was made on one of the specimens. The temperature at the start of the run was approximately 3000°C. The flow rate of CO_2 injected into the argon plasma was 22 mg/sec and the duration of the CO_2 flow was 60 sec. The complexities associated with the degree of dissociation of the gases, temperature distributions, heat transfer considerations, and possible boundary layer effects will be discussed in the final report.

The average maximum surface recession rate ($\dot{\Delta}r$) was 0.23 mil sec^{-1} and the average mass erosion rate ($\dot{\Delta}m$) was 7.6 mg sec^{-1}. This $\dot{\Delta}r$ value of 0.23 mil sec^{-1} lies somewhat below the previously determined range of 0.27 to 0.33 mil sec^{-1} for fg-pss W*, cg-pss W*, and W + 2% Th at this flow rate. The $\dot{\Delta}m$ of 7.6 mg sec^{-1} is, however,

*fg-pss: fine grain-pressed, sintered and swaged. cg-pss: coarse grain-pressed, sintered and swaged.

Copy No. ____

greater than the corresponding range of 5.0 to 6.0 mg sec^{-1} for the other three types of W. The lesser value of $\dot{\Delta}r$ for the Ag-infiltrated W is attributed to Ag boiling off and presenting a partial barrier between the CO_2 and the W. Likewise, the higher mass erosion rate ($\dot{\Delta}m$) is most likely caused by the evaporation of Ag.

After the run the specimen surface was dull and gray as opposed to the shiny "electropolished" appearance of the pure W specimens (fg-pss, cg-pss). A longitudinal section of the specimen is being metallographically prepared to measure the Ag depletion. Runs at higher CO_2 flow rates will be made when sufficient samples are available.

Erosion of fg-pss W by Al_2O_3

Two preliminary runs (A and B) were made with desiccator-stored 280 grit Al_2O_3. The Al_2O_3 flow rate to the plasma in Run A was between 6 and 12 gm min^{-1} and for Run B between 1 and 6 gm min^{-1}. These flow rates are not known more precisely because of lack of reproducibility with the powder feed mechanism. In the future, the actual weight loss of Al_2O_3 from the canister will be measured.

Run A was a very preliminary run; temperatures were comparable to those in Run B but the exposure time of the W specimen to the Al_2O_3 in the plasma was shorter.

In Run B a 2-color pyrometer was used to measure and record specimen temperature. Also, a relatively successful motion picture of a projected and magnified image of the W specimen being struck by the Al_2O_3-containing plasma was obtained.

The Al_2O_3 was introduced into the plasma for intermittent periods of 60, 65, and 80 seconds and the specimen was heated after each period by the argon plasma alone for intervals of 150, 120, and 15 seconds respectively. The specimen temperature in argon alone was approximately 2900°C. Then the Al_2O_3 was introduced, the specimen surface temperature dropped to approximately 2500°C and remained at this value until the Al_2O_3 was shut off; it then returned to approximately 2900°C.

The motion picture revealed that a molten film of Al_2O_3 blown across the specimen area of direct plasma impingement and collected as droplets above and below this area and on the back side of the specimen. Also, some Al_2O_3 from the top region was observed to flow down the back side. Al_2O_3 in all three regions is shown in Fig. 1, which is a still photograph from the motion picture. The Al_2O_3 was found to grow in large deposits on the colder portions of the specimen. These deposits can be observed in Fig. 2, which is a photograph of the specimen after the completion of Run A.

As can be seen in Fig. 3, the plasma impingement surface of the specimens was more dull and gray than the original centerless-ground-finish, while the portion of the back surface which had been underneath

the Al_2O_3 deposits had an "electropolished" appearance similar to that observed in the CO_2 experiments. Also, metallic W was found deposited in voids in the Al_2O_3 bead on the back surface. Both the W-transport and the "electropolished" surface were also noted in previous work[1] on this project on static reactions between W and Al_2O_3. In that investigation a W cap was found on the Al_2O_3. Apparently similar results (Fig. 2) can be noted on the Al_2O_3 deposits in the present study. Further metallographic work is being reserved for the runs with specially dried Al_2O_3. It is of interest that the erosion run combined dynamic and quasi-static reaction conditions for W and Al_2O_3. On the plasma impingement surface, the Al_2O_3 struck the W with considerable velocity and then (except perhaps for a thin film) was swept away from the interface. On the back side, W is contacted by the relatively stagnant and probably cooler Al_2O_3 bead. These back side conditions are essentially those employed in the aforementioned static study, so the similarity in results should not be surprising.

Surface recession measurements were made after the Al_2O_3 deposits had been chipped away. The maximum surface recession was 2-1/2 and 5 mils on the plasma impingement side and 1-1/2 and 3 mils on the back side for Runs A and B respectively. Taking the front recession alone and counting only the period of Al_2O_3 impingement as reaction time, the average maximum surface recession rate ($\Delta\dot{r}$) for Run B was: $\Delta\dot{r} = \frac{5}{60 + 65 + 80} = 0.024$ mil sec^{-1}.

For the CO_2 experiments the range of $\Delta\dot{r}$ was: $\Delta\dot{r} = 0.1$ mil sec^{-1} for CO_2 flow rate = 7 mg sec^{-1} to $\Delta\dot{r} = 0.7$ mil sec^{-1} for CO_2 flow rate = 90 mg sec^{-1}.

Thus, for the conditions studied to date, the surface recession rate of W in Al_2O_3 is much lower than for erosion of W by CO_2.

In preparation for future runs, a quantity of 280 grit Al_2O_3 was heated at 1000°C in vacuum for 3 hours to drive off surface contaminants. This Al_2O_3 was transferred to a Mason jar in an evacuated and argon-backfilled dry box, and the Mason jar stored in the dry box.

Thermal Shock Study

A third series of W cylinders (85% dense, pressed and sintered) was fabricated for use as mechanical-property specimens and will be sent to Aerojet-General Corporation, Azusa, for testing.

The effects of cylinder wall thickness and OD/ID ratio on the magnitude and time variation of thermal stress are currently under study. A series of four W specimens received from Aerojet-General Corporation (made from 99.6% dense, 1/4-inch thick, Universal Cyclops recrystallized plate) were subjected to similar thermal environments in the thermal shock apparatus. Chromel-Alumel thermocouples were attached to

1. A. Neiman, O. Preston and D. Brown, "Tungsten and Rocket Motors," Final Report, Contract No. NOrd-18619(FBM), March 23, 1961.

the outside surface of each specimen and the outer surface temperature was recorded continuously during each run. In addition, the graphite heater surface temperature and the outer circumferential strain were recorded. Due to the relatively small inside diameter of the specimens (1/2 inch) it was not practical to use a shutter such as described in the previous progress report. Consequently, as may be seen in Fig. 4, there was a slight time delay of about 2 seconds before the heater reached its quasi-steady-state temperature of 3000°C. The heater maintained this temperature for the remaining 5 seconds of the runs. The outer specimen surface temperature is also shown plotted versus time in Fig. 4. As expected, the temperature rise was inversely related to the specimen wall thickness. The maximum temperature recorded was limited by the melting point of the Chromel-Alumel thermocouples.

The total outer circumferential strain, Fig. 5, was found to vary with time and specimen dimensions in the same manner as the specimen temperature. The maximum total strain rates generated during the four tests were $2.32 \times 10^{-3} sec^{-1}$, $1.57 \times 10^{-3} sec^{-1}$, $0.44 \times 10^{-3} sec^{-1}$, and $0.20 \times 10^{-3} sec^{-1}$, respectively, for the 0.72-inch OD, 0.93-inch OD, 1.44-inch OD, and 1.94-inch OD cylinders.

The "effective" outer circumferential strain* is shown versus time in Fig. 6. Unfortunately, at the relatively low heat flux obtainable for these 1/2-inch ID specimens, the thermally generated effective strains approach the limit of experimental accuracy for the dynamic strain measurement technique employed. This limit corresponds to an estimated average error of $\pm 1 \times 10^{-4}$ inches in the diameter displacement measurement. Thus, for example, a 2-inch diameter cylinder could have a strain error of $\pm 5 \times 10^{-5}$ in./in. However, even with this possible error there seems to be a definite trend in Fig. 6 with respect to curve shape and locus of maxima. The "effective" strain rises rapidly to a maximum and then drops off more gradually with increasing time. Both the magnitude of the maximum effective strain and the time required to reach it increase with increasing wall thickness and OD/ID. The outer circumferential stress, Fig. 7, was calculated for this series of runs using the relationships discussed in the previous progress report. The stress varies with time, wall thickness, and OD/ID in a very similar manner to the "effective" strain, the difference being due to the temperature variation of the elastic modulus. The maximum stress developed (about 13,000 psi) occurred in the 1.94-inch OD cylinder and was far below the ultimate tensile stress for the high density material tested. In the case of the 0.72-inch OD specimen (0.11-inch wall) no measurable stress was detected. It is interesting to note, however, that in each case, the maximum stress occurred before the outside surface temperature exceeded 200°F. Thus, the estimated ductile-brittle transition temperature of 400-600°F was not exceeded, and if the stress had been sufficiently high, the material would have failed in a brittle manner. It is therefore apparent that

*The "effective" outer strain is equal to the total outer strain minus the outer thermal expansion strain.

transition temperature is among the most important factors determining the thermal shock resistance of W. This conclusion is further supported by recently published data[2] on the effects of surface finish on transition temperature. It was reported that preoxidized W had a considerably lower transition temperature and that forged W rocket components (given such a preoxidation treatment) possessed significantly better thermal shock resistance.

Thermal shock tests were also performed on several series of ceramic cylinders in an attempt to further correlate the effects of cylinder wall thickness on thermal shock resistance. The ceramic (Norton RA 98 Alundum) was selected because of the ease and reproducibility with which thermal shock cracks can be generated in this material. However, the ceramic material does possess a much lower thermal conductivity than W and any comparisons of results obtained on the two materials should be made cautiously. The ceramic specimens were all machined from one thick-walled tube (2-3/4-inch OD x 2-inch ID) so as to possess similar mechanical and physical properties. For each thermal shock test run, a series of five to seven specimens were stacked concentric with a 1-inch OD graphite heater. The specimens were all 2-inch ID x 1/2-inch high and the wall thicknesses varied in 1/16-inch intervals, as indicated in Table I. Due to the relatively high heat fluxes normally generated in the thermal shock apparatus, it was difficult to prevent all of the specimens from cracking. However, by lowering the heat-up rate for each successive test run, it was possible to find a power setting at which all but the very thinnest cylinders (1/16-inch wall) cracked. Mirrors were placed behind the specimen so that almost the entire perimeter could be photographed and movies were taken of each test run. It was possible from these to see the cracks forming suddenly in the thicker specimens. The cracks appeared as bright lines due to the contrast between the relatively hot heater and the colder outside specimen surface. With the thinner specimens (1/16- and 1/8-inch wall) the brightness difference between the heater and the outside specimen surface was not sufficient (due to specimen translucency) to outline the cracks except for the very lowest heat-flux run (No. 5) where crack formation in the 1/8-inch wall was observed. Cracks in the 1/16-inch wall could not be observed except near the end of the runs when a filter was placed in front of the camera lens. In future runs, the filter will be used during the entire run. Only at the lowest heat-up rate employed (run No. 5) was it possible to obtain uncracked specimens after the run. In this case, the two 1/16-inch wall specimens remained uncracked. One of the uncracked specimens plus the other cracked cylinders are shown in Fig. 8. Although there was some scatter in the chronological sequence of crack formation during the five runs (probably due to flaws in the ceramic) there was a definite trend. It appears that the maximum stress generated is less in the thinner cylinders and that the time to reach a given stress below the maximum increases with increasing wall thickness.

---

2. E. A. Steigerwald and G. J. Guarnieri, "Influence of Surface Oxidation on the Brittle-to-Ductile of Tungsten," Trans. ASM, 55, 307, No. 2, June 1962. Discussion: P. McAllister, Trans. ASM, 55, 1056, No. 4, December 1962.

A schematic plot of the type of stress-time relationship implied by the data is presented in Fig. 9 for run No. 5. This same general type of behavior appears to also hold for W, Fig. 7. However, although a trend appears to be established, considerably more data must be obtained before any firm conclusions can be drawn on the effects of wall thickness and OD/ID on the magnitude and time variation of thermal stresses in W and other potential nozzle materials. Future tests on W will be performed at higher heat fluxes and where feasible with a radiation shutter present. Also, an attempt will be made to employ the motion picture technique for detection of cracks in W.

Future Work

In the next reporting period the study of W erosion by Al_2O_3 will be continued. The erosive effect of other exhaust constituents will also be investigated.

Work is continuing on the preparation of additional mechanical-property specimens of 90 and 95% density and of wrought material. Further thermal shock testing of W specimens of variable dimensions and various types is planned.

Gerald M. Gordon
Senior Metallurgist

David A. Brown
Metallurgist

Approved:

A. E. Gorum, Director
Material Sciences Division

Table I

DATA TAKEN FROM MOVIES ON FIVE THERMAL SHOCK TEST RUNS MADE ON 2-INCH ID x 1/2-INCH HIGH, NORTON RA 98 ALUNDUM SPECIMENS

Run Number	1	2	3	4	5
Wall Thicknesses of Specimens Present (in 1/16-inch units)	2, 3, 4, 5, 6	1, 2, 3, 4, 5, 6	1, 2, 3, 4, 5, 6	1, 2, 3, 4, 5, 6	1, 1, 2, 3, 4, 5, 6
Approximate Heater Temperature (^{o}C) at End of 10 Seconds	2800	2500	2200	2200	700
Duration of Run (seconds)	15	33	18	10	45
[1]Specimen Wall Thicknesses in Observed Chronological Order of Cracking (in 1/16-inch units)	5, 6	3, 4, 5, 6	3, 4, 5, 6	$\overset{\frown}{3, 2}$, $\overset{\frown}{5, 4}$, 6	4, $\overset{\frown}{3, 2}$, 5, 6
Specimens Found Uncracked After Run	none	none	none	none	1, 1

1. The symbol ($\frown$) placed over two specimen numbers indicates that cracking occurred almost simultaneously.

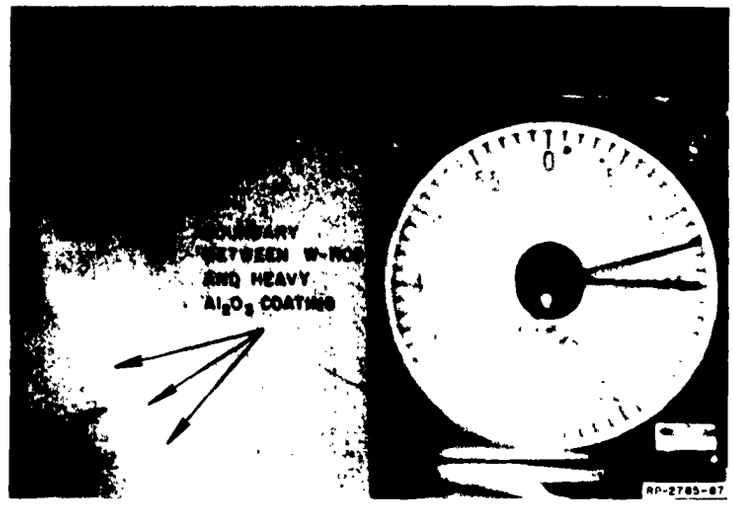

FIG. 1 PHOTOGRAPH FROM MOTION PICTURE OF W-Al_2O_3 EROSION RUN

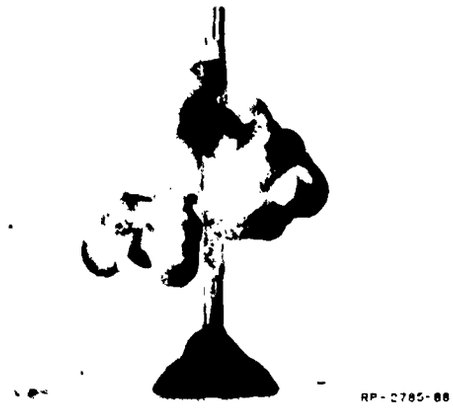

FIG. 2 PHOTOGRAPH OF W SPECIMEN AFTER RUN A

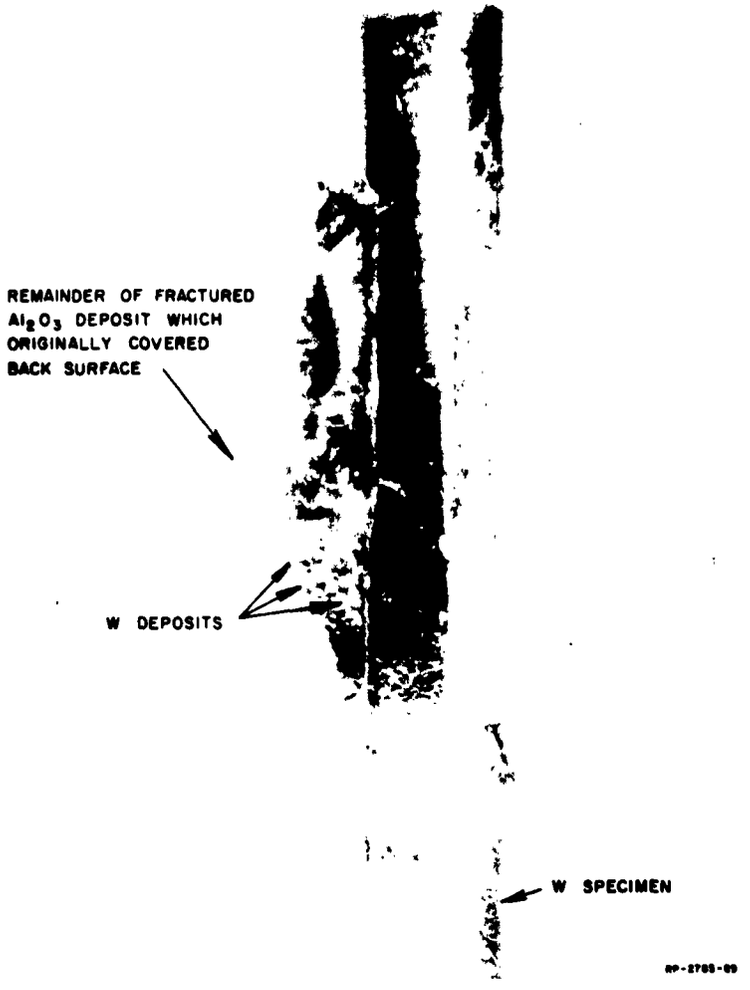

FIG. 3 PHOTOGRAPH OF W SPECIMEN – RUN B

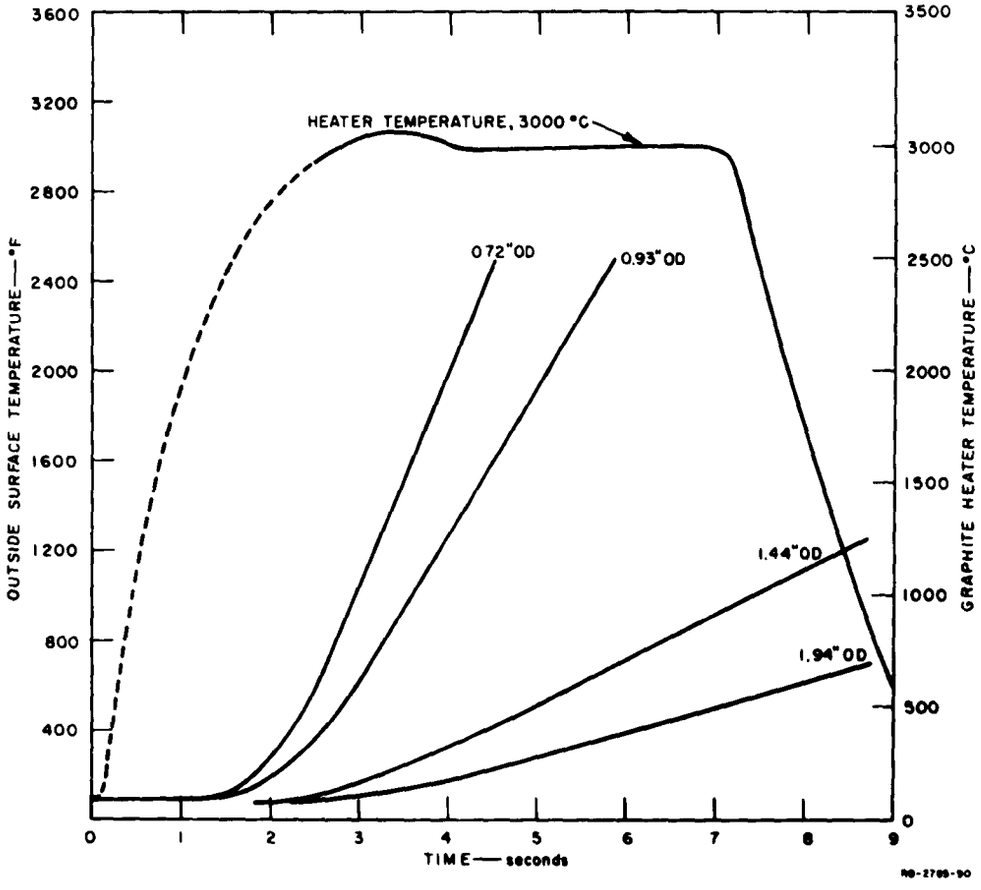

FIG. 4 GRAPHITE HEATER TEMPERATURE AND OUTER SURFACE TEMPERATURE vs. TIME FOR A SERIES OF TUNGSTEN PLATE SPECIMENS (99.6% dense, ½ inch ID × ¼ inch high) OF VARYING WALL THICKNESS

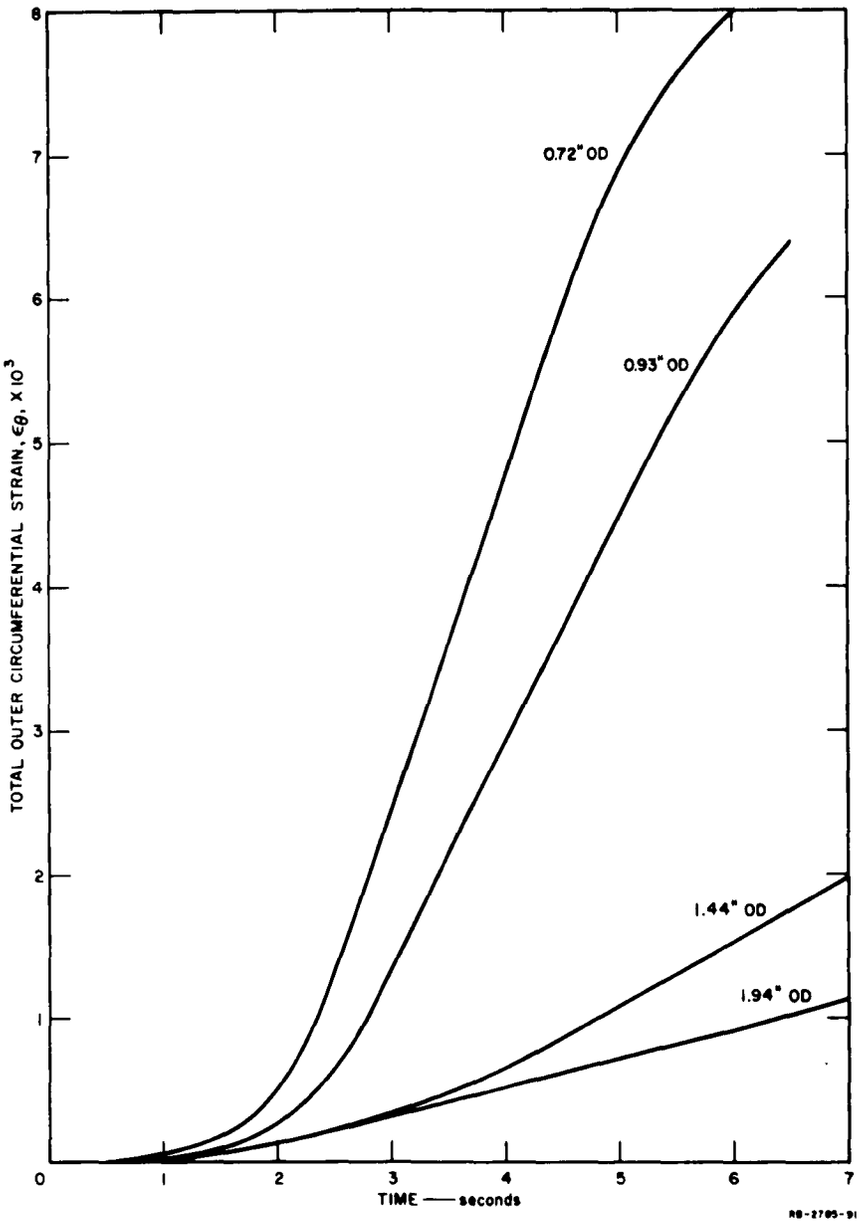

FIG. 5 EFFECT OF WALL THICKNESS ON THE TOTAL OUTER CIRCUMFERENTIAL STRAIN FOR A SERIES OF TUNGSTEN PLATE SPECIMENS (99.6% dense, ½ inch ID × ¼ inch high)

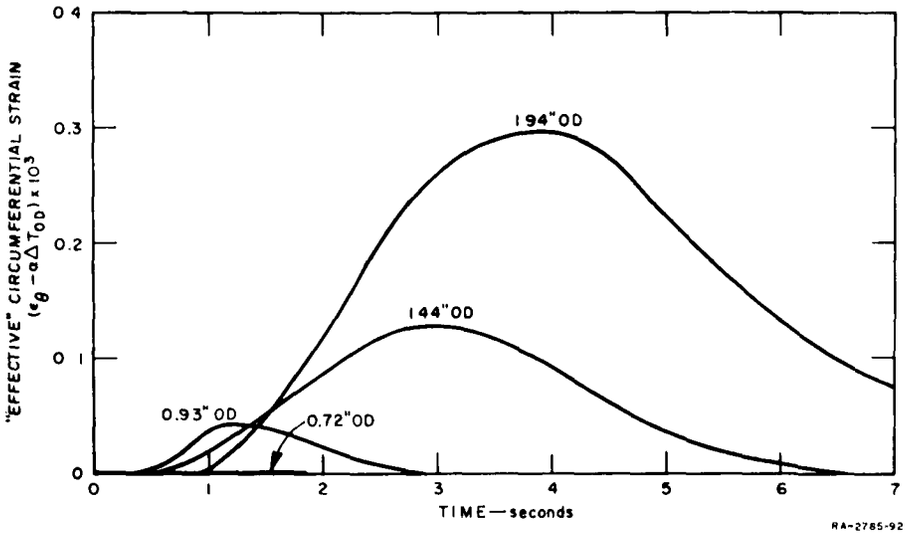

FIG. 6 EFFECT OF WALL THICKNESS ON THE "EFFECTIVE" OUTER CIRCUMFERENTIAL STRAIN FOR A SERIES OF TUNGSTEN PLATE SPECIMENS (99.6% dense, ½ inch ID × ¼ inch high)

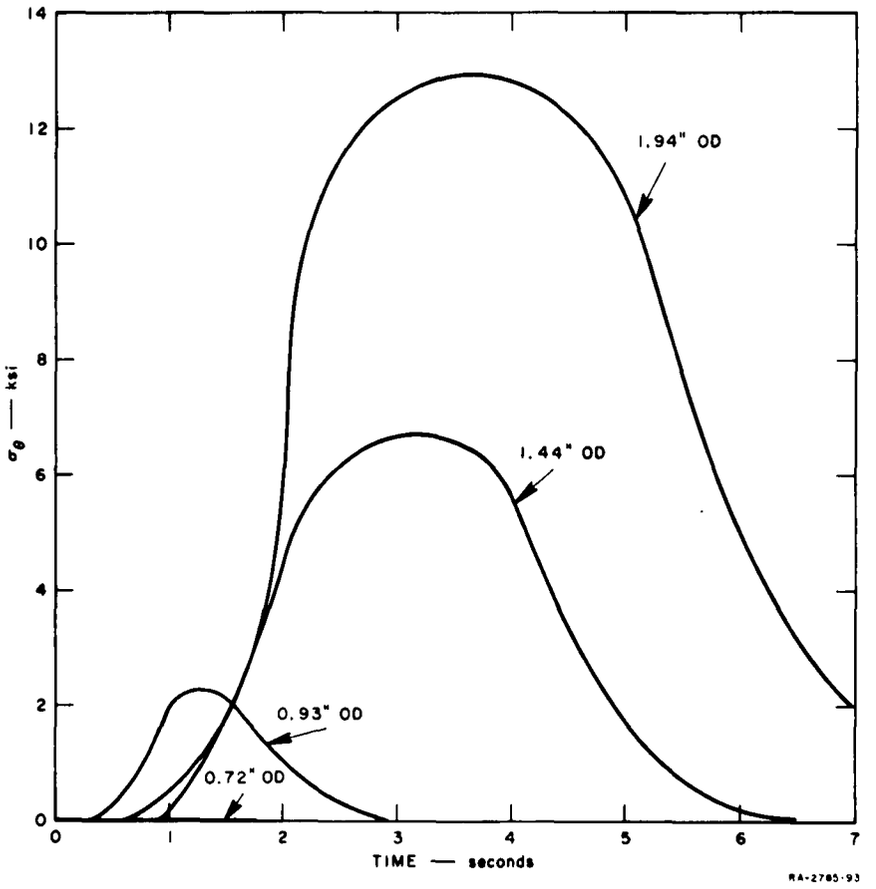

FIG. 7 EFFECT OF WALL THICKNESS ON THE OUTER CIRCUMFERENTIAL THERMAL STRESS FOR A SERIES OF TUNGSTEN PLATE SPECIMENS (99.6% dense, ½ inch ID × ¼ inch high)

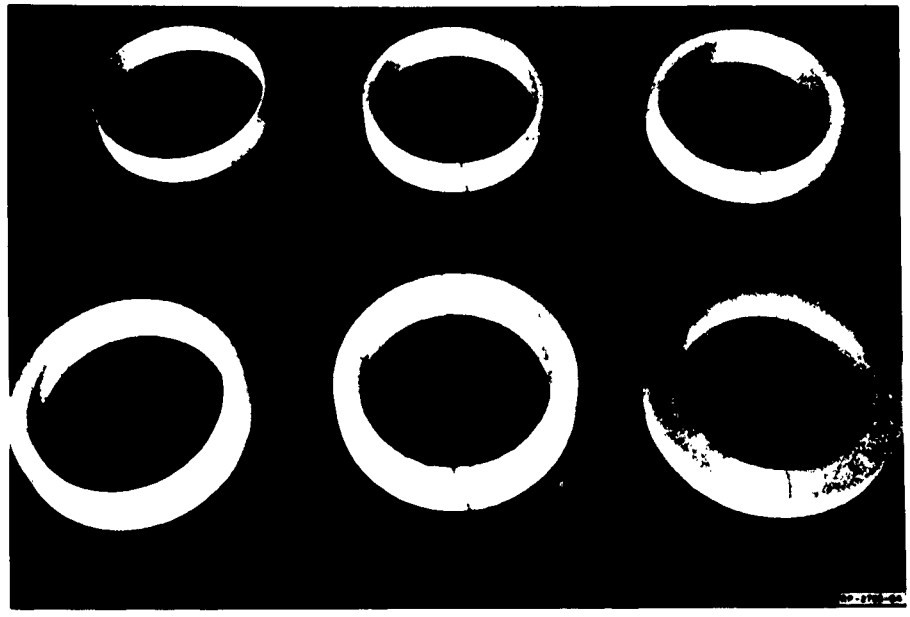

FIG. 8 PHOTOGRAPH OF ONE OF THE UNCRACKED CERAMIC SPECIMENS PLUS THE OTHER CRACKED CYLINDERS FROM RUN 5

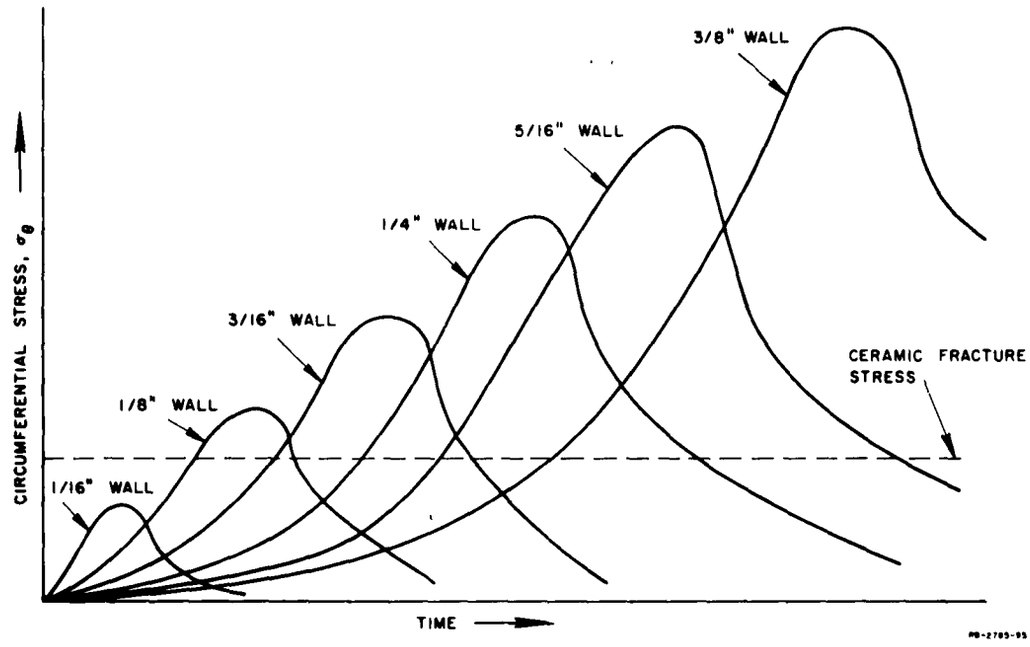

FIG. 9 SCHEMATIC OF STRESS-TIME-WALL THICKNESS RELATIONSHIP IMPLIED FROM CERAMIC RUN NO. 5